

2

NAVAL POSTGRADUATE SCHOOL

Monterey, California

AD-A247 149



THEESIS

DTIC
ELECTED
MAR 10 1992
SBD

TESTING THE ACCURACY OF A THREE-DIMENSIONAL ACOUSTIC COUPLED MODE MODEL

by

Hiroyuki Ogawa

December 1991

Thesis Advisor:

Thesis Co-Advisor:

Ching-Sang Chiu

Laura L. Ehret

Approved for public release; distribution is unlimited.

6 0 0 0 0 0 149 149

92-06195



UNCLASSIFIED

SECURITY CLASSIFICATION OF THIS PAGE

REPORT DOCUMENTATION PAGE

Form Approved
OMB No. 0704-0188

1a REPORT SECURITY CLASSIFICATION UNCLASSIFIED		1b. RESTRICTIVE MARKINGS	
2a. SECURITY CLASSIFICATION AUTHORITY		3. DISTRIBUTION /AVAILABILITY OF REPORT Approved for public release; distribution is unlimited.	
2b. DECLASSIFICATION/DOWNGRADING SCHEDULE			
4. PERFORMING ORGANIZATION REPORT NUMBER(S)		5. MONITORING ORGANIZATION REPORT NUMBER(S)	
6a. NAME OF PERFORMING ORGANIZATION Naval Postgraduate School		6b. OFFICE SYMBOL (If applicable) 35	7a. NAME OF MONITORING ORGANIZATION Naval Postgraduate School
6c. ADDRESS (City, State, and ZIP Code) Monterey, CA 93943		7b. ADDRESS (City, State, and ZIP Code) Monterey, CA 93943	
8a. NAME OF FUNDING/SPONSORING ORGANIZATION		8b. OFFICE SYMBOL (If applicable)	9. PROCUREMENT INSTRUMENT IDENTIFICATION NUMBER
8c. ADDRESS (City, State, and ZIP Code)		10. SOURCE OF FUNDING NUMBERS	
		PROGRAM ELEMENT NO.	PROJECT NO.
		TASK NO.	WORK UNIT ACCESSION NO.

11. TITLE (Include Security Classification)

*Testing the Accuracy of a Three-dimensional Acoustic Coupled Mode Model*12 PERSONAL AUTHOR(S)
Hiroyuki Ogawa13a TYPE OF REPORT
Master's thesis 13b. TIME COVERED
FROM _____ TO _____14. DATE OF REPORT (Year, month day)
December, 199115. PAGE COUNT
56

16. SUPPLEMENTARY NOTATION

17. COSATI CODES

FIELD	GROUP	SUB-GROUP

18. SUBJECT TERMS (Continue on reverse if necessary and identify by block number)

Ocean acoustics; normal mode; parabolic equation

19 ABSTRACT (Continue on reverse if necessary and identify by block number)

The three-dimensional coupled mode sound propagation model of Chiu and Ehret (1990) is tested for its accuracy in modeling horizontal sound refraction. This test is achieved by comparing results generated by this model with exact analytic solutions to a parabolic approximation of the Helmholtz Equation (Seigmann et al., 1990). Specifically, the acoustic wavefields associated with two cases of horizontally variable sound speed are considered. In Case I the sound speed varies only with azimuth, while in Case II there is radial and azimuth variation. The acoustic quantities used for the comparison include the modal modulation envelopes and transmission loss. Errors in the mode amplitude and phase are quantified and the significance of horizontal refraction is discussed.

20. DISTRIBUTION/AVAILABILITY OF ABSTRACT

X UNCLASSIFIED/UNLIMITED SAME AS RPT.

DTIC USERS

21. ABSTRACT SECURITY CLASSIFICATION

UNCLASSIFIED

22a. NAME OF RESPONSIBLE INDIVIDUAL

Dr. Ching-Sang Chiu

22b. TELEPHONE (Include Area Code)

(408) 646-3239

2c. OFFICE SYMBOL

OC/Ci

Approved for public release; distribution is unlimited

**TESTING THE ACCURACY OF A
THREE-DIMENSIONAL ACOUSTIC COUPLED MODE MODEL**

by

Hiroyuki Ogawa

Lieutenant Commander, Japan Maritime Self-Defence Force
B.S., National Defence Academy of Japan, 1977

Submitted in partial fulfillment of the requirements for the degree of
MASTER OF SCIENCE IN PHYSICAL OCEANOGRAPHY

From the

NAVAL POSTGRADUATE SCHOOL
December 1991

Author:

Hiroyuki Ogawa
Hiroyuki Ogawa

Approved by:

Ching-Sang Chiu
Ching-Sang Chiu, Thesis Advisor

Laura L. Ehret
Laura L. Ehret, Thesis Co-Advisor

Curtis A. Collins
Curtis A. Collins, Chairman
Department of Oceanography

ABSTRACT

The three-dimensional coupled mode sound propagation model of Chiu and Ehret (1990) is tested for its accuracy in modeling horizontal sound refraction. This test is achieved by comparing results generated by this model with exact analytic solutions to a parabolic approximation of the Helmholtz Equation (Seigmann et al., 1990). Specifically, the acoustic wavefields associated with two cases of horizontally variable sound speed are considered. In Case I the sound speed varies only with azimuth, while in Case II there is radial and azimuth variation. The acoustic quantities used for the comparison include the modal modulation envelopes and transmission loss. Errors in the mode amplitude and phase are quantified and the significance of horizontal refraction is discussed.

CONFIDENTIAL

Accession For	
NTIS GRA&I	<input checked="" type="checkbox"/>
DTIC TAB	<input type="checkbox"/>
Unannounced	<input type="checkbox"/>
Justification	
By _____	
Distribution/ _____	
Availability Codes	
Dist	Avail and/or Special
A-1	

TABLE OF CONTENTS

I. INTRODUCTION	1
II. ANALYSIS AND METHOD OF MODEL COMPARISON	3
A. INDEX OF REFRACTION	5
1. Case I	5
2. Case II	5
B. ENVELOPE FUNCTION	6
III. MODEL RUNS	12
IV. RESULTS	14
A. CASE I	14
B. CASE II	18
V. DISCUSSION	26
A. HORIZONTAL REFRACTION	26
B. ACCURACY	27
1. Phase	27
2. Amplitude	28
3. Transmission Loss (TL)	28
VI. CONCLUSIONS	29
APPENDIX	30
REFERENCES	42
INITIAL DISTRIBUTION LIST	44

LIST OF TABLES

TABLE 1. THE AZIMUTH AND RADIAL SOUND SPEED VARIATION.....	12
TABLE 2. PHASE DIFFERENCE.....	27
TABLE 3. AMPLITUDE DIFFERENCE	28
TABLE 4. TRANSMISSION LOSS DIFFERENCE.....	28

LIST OF FIGURES

Figure 1. Case I Sound Speed Field for $\alpha_0 = 0.005$ and $C_0 = 1500$ m/s.....	7
Figure 2. Case II Sound Speed Field for $\alpha_0 = 4 \times 10^{-7}$ and $C_0 = 1500$ m/s	7
Figure 3. Amplitude of U_{NM} for Case I with $\alpha = 0.005$ and $\beta = 0.1$	15
Figure 4. Phase of U_{NM} for Case I with $\alpha = 0.005$ and $\beta = 0.1$	15
Figure 5. Amplitude of U_{PE} , for Case I with $\alpha = 0.005$ and $\beta = 0.1$	16
Figure 6. Phase of U_{PE} for Case I with $\alpha = 0.005$ and $\beta = 0.1$	16
Figure 7. Amplitude Difference in Percent for Case I with $\alpha = 0.005$ and $\beta = 0.1$	17
Figure 8. Phase Difference in Degree for Case I with $\alpha = 0.005$ and $\beta = 0.1$...	17
Figure 9. TL_{NM} at a Depth of 1000 m for Case I with $\alpha = 0.005$ and $\beta = 0.1$...	19
Figure 10. TL_{PE} at a Depth of 1000 m for Case I with $\alpha = 0.005$ and $\beta = 0.1$	19
Figure 11. Difference in TL in dB for Case I with $\alpha = 0.005$ and $\beta = 0.1$	20
Figure 12. Amplitude of U_{NM} for Case II with $\alpha = 4 \times 10^{-7}$ and $\beta = 0.1$	21
Figure 13. Phase of U_{NM} for Case II with $\alpha = 4 \times 10^{-7}$ and $\beta = 0.1$	21
Figure 14. Amplitude of U_{PE} for Case II with $\alpha = 4 \times 10^{-7}$ and $\beta = 0.1$	22
Figure 15. Phase of U_{PE} for Case II with $\alpha = 4 \times 10^{-7}$ and $\beta = 0.1$	22
Figure 16. Amplitude Difference in Percent for Case II with $\alpha = 4 \times 10^{-7}$ and $\beta = 0.1$	23
Figure 17. Phase Difference in Degree for Case II with $\alpha = 4 \times 10^{-7}$ and $\beta = 0.1$	23
Figure 18. TL_{NM} at a Depth of 1000 m for Case II with $\alpha = 4 \times 10^{-7}$ and $\beta = 0.1$	24
Figure 19. TL_{PE} at a depth of 1000 m for Case II with $\alpha = 4 \times 10^{-7}$ and $\beta = 0.1$...	24
Figure 20. Difference in TL in dB for Case II with $\alpha = 4 \times 10^{-7}$ and $\beta = 0.1$	25
Figure 21. Phase of U_{NM} for N×2D for Case I with $\alpha = 0.005$ and $\beta = 0.1$	27

LIST OF NOTATION

A :	the coefficient of eigenfunction
A_p :	the amplitude of the envelope function for PE
$C(\bar{r})$:	the sound speed as a function of position \bar{r}
C_0 :	the reference sound speed
$D_n, E_n, F_n, \tilde{G}_{mn}, H_{mn}$:	the coefficients in the equation for normal mode envelope function
H :	ocean depth
$H_0^1(k_0 r)$:	zeroth order Hankel function of the first kind
$k(\bar{r})$:	the acoustic wave number
k_n :	the corresponding horizontal wavenumber (eigenvalue)
$n(\bar{r})$:	index of refraction
$P(\bar{r}, t)$:	the acoustic pressure
$P_n(r, \theta)$:	the mode amplitude function at point (r, θ) for normal mode theory
Φ_{NM} :	an acoustic pressure for numerical normal mode
Φ_{PE} :	an acoustic pressure for analytic PE
$q(\bar{r}, t)$:	an acoustic source
\bar{r} :	position vector of function (r, θ, z)
r :	radial range
t :	time
TL :	transmission loss
$u(r, \theta, z)$:	modulation on PE
$U_1(r, \theta)$:	analytic envelope function associated with Mode 1
U_n :	envelope function for normal mode
U_p :	envelope function for PE
$v(r)$:	rapidly varying portion for PE
U_n^i	envelope function at the i^{th} iteration for mode n
f :	acoustic frequency
\hat{r} :	the unit directional vectors in r

TL_{NM} :	the numerical NM transmission loss
TL_{PE} :	the analytic PE transmission loss
$Z_n(r, \theta)$:	n^{th} local normal mode (eigenmode) at point (r, θ)
α_0, β_0 :	arbitrary constants
γ_j :	vertical wavenumber of the j^{th} mode
$\gamma_{mn}, \beta_{mn}, B_{mn}$:	mode coupling coefficients
Θ :	phase of the PE envelope function
θ :	azimuth angle
$\Phi(\tilde{r})$:	the time-independent acoustic pressure component
ϕ_n :	range integral of horizontal wavenumber
w :	circular frequency
$\hat{\theta}$:	the unit directional vector in θ
z :	depth

ACKNOWLEDGEMENT

I would like to thank my thesis advisors, Professors Chiu and Ehret for inviting me to join in their research. Their excellent guidance and patient counsel enabled me to understand and use the (new) concepts of ocean acoustics. Without their consultation and assistance my thesis would not have been possible.

I would also like to thank Mrs. Hania La Born for her help in thesis typing and Mr. Stephen J. Foreman for his help in thesis editing.

Finally, I would like to thank my wife, Hiromi, for her support and understanding during the semester of this thesis.

L INTRODUCTION

The field of three-dimensional (3D) underwater acoustics has been developed in an attempt to describe the properties and characteristics of sound propagation in the heterogeneous ocean environment (Lynch and Chiu, 1989). At present, there are three major approaches used in studying the 3D underwater sound field. One of these, ray theory, is premised upon a high-frequency approximation method. This method gives a geometric-optics solution which involves ray-tracing in a spatially varying sound speed field. The Hamiltonian Acoustic Ray Tracing Program for the Ocean (HARPO) is a versatile numerical code developed by Jones et al. (1986) for the computation of 3D rays. The primary deficiency of this theory is that it cannot adequately address the behavior of low-frequency sound due to the neglect of sound dispersion and diffraction.

The second approach uses a parabolic approximation to the acoustic wave equation, which was introduced by Tappert (1977). A 3D numerical parabolic equation (PE) model was developed by Lee et al. (1988) using an implicit finite difference scheme. Another 3D PE model was arrived at by Baer (1981) utilizing a split-step Fourier algorithm. In a recent study, analytic solutions to the 3D parabolic equation were obtained by Seigmann et al., (1990). These solutions are valuable for testing the accuracy of 3D numerical models.

A third approach is the normal mode method. Pierce presented a three-dimensional version of this method in 1965. The normal mode method is based upon a separable solution to the wave equation. Pierce assumed an adiabatic acoustic environment which leads to the neglect of coupling

presented by Chiu and Ehret (1990). This later 3D normal mode model accounts for both horizontal refraction and model coupling.

Any improvement in acoustic modeling must be quantified. We shall endeavor to test the accuracy of the 3-D coupled normal mode model of Chiu and Ehret (1990) in regard to horizontal refraction.

To examine the accuracy of the Chiu-Ehret model, we compare the results of their model with those from analytic solutions to the parabolic equation arrived at by Seigmann, et al. (1990). The results of the Chiu-Ehret model and the analytic solutions of the parabolic equation are compared for two cases of horizontal variation in sound speed. As a means of comparing the results, we examine the slow variations of the complex pressure envelope function and transmission loss.

Our simulated acoustic field has a range of 100 km with azimuth from 30° to 180° . Two variations in the horizontal sound speed field were used. In Case I the sound speed varies only with the azimuth angle while Case II varies both with the azimuth and radial.

The normal mode theory used by Chiu and Ehret is described in detail in the Appendix. The appendix also includes a description of the PE approximation and the analytic solutions developed by Seigmann et al. (1990).

II. ANALYSIS AND METHOD OF MODEL COMPARISON

The three-dimensional coupled normal mode model was applied to two sound speed fields for which exact analytic solutions to the PE approximation are available. These analytic PE solutions for vertically invariant sound speed were developed by Seigmann et al. (1990). Their development was based on expressing the "time-independent" acoustic pressure component as

$$\Phi_{PE}(r, \theta, z) = U_p(r, \theta) \sin(\gamma_j z) \exp \left\{ -\frac{ik_0 r}{2} \left(\frac{\gamma_j}{k_0} \right)^2 \left[1 - \frac{1}{4} \left(\frac{\gamma_j}{k_0} \right)^2 \right] \right\} \times \left(\frac{2}{\pi k_0 r} \right)^{\frac{1}{2}} \exp \left[i \left(k_0 r - \frac{\pi}{4} \right) \right]$$

where

$$k_0 = \frac{2\pi f}{C_0}$$

$$\gamma_j = \left[j + \frac{1}{2} \right] \frac{\pi}{H} \quad (j = 0, 1, 2, \dots)$$

C_0 = reference sound speed

f = acoustic frequency

H = ocean depth.

The reduced complex envelope function

$$U_p(r, \theta) = A_p(r, \theta) \exp \{ i\Theta(r, \theta) \}$$

U_p is governed by

$$\frac{\partial U_p}{\partial r} = \frac{ik_0}{2} \left\{ \left(n^2 - 1 \right) \left[1 + \frac{1}{2} \left(\frac{\gamma_j}{k_0} \right)^2 \right] - \frac{1}{4} \left(n^2 - 1 \right) - \frac{1}{2} \left(\frac{\gamma_j}{k_0} \right)^4 + \frac{1}{(k_0 r)^2} \frac{\partial^2}{\partial \theta^2} \right\} U_p \quad (2.1)$$

where

$$n(\vec{r}) = \frac{C_0}{C(\vec{r})} \quad (\vec{r} = (r, \theta, z))$$

$C(\vec{r})$ = sound speed as a function of position \vec{r} .

Substitution and separation of real and imaginary parts gives two coupled equations governing A_p and Θ :

$$\frac{\partial A_p}{\partial r} + \frac{1}{k_0 r^2} \frac{\partial A_p}{\partial \theta} \frac{\partial \Theta}{\partial \theta} + \frac{A_p}{2k_0 r^2} \frac{\partial^2 \Theta}{\partial \theta^2} = 0 \quad (2.2)$$

$$\begin{aligned} & \left(n^2 - 1 \right) \left[1 + \frac{1}{2} \left(\frac{\gamma_j}{k_0} \right)^2 \right] - \frac{1}{4} (n^2 - 1)^2 - \frac{1}{2} \left(\frac{\gamma_j}{k_0} \right)^4 \\ & = \frac{2}{k_0} \frac{\partial \Theta}{\partial r} + \frac{1}{(k_0 r)^2} \left(\frac{\partial \Theta}{\partial \theta} \right)^2 - \frac{1}{(k_0 r)^2} \frac{1}{A_p} \frac{\partial^2 A_p}{\partial \theta^2}. \end{aligned} \quad (2.3)$$

If one chooses $\Theta(r, \theta) = \alpha(r)\theta$, equation (2.2) may be solved for the amplitude, i.e.,

$$A_p(r, \theta) = F \left[\theta - \frac{1}{k_0} \int \frac{\alpha(s)}{s^2} ds \right]. \quad (2.4)$$

Choosing $\alpha(r)$ and the functional dependence F results in a reduced envelope function (and ultimately acoustic pressure) while equation (2.3) can be solved for the index of refraction $n(\vec{r})$ and thus the sound speed field $C(\vec{r})$. Equation (2.3) is for a wide angle PE approximation. This wide angle form will be used throughout. To judge the accuracy of the Chiu-Ehret model in calculating horizontal refraction we compare the numerical coupled mode results with the analytic PE results for two sound speed fields or two functional definitions of $\alpha(r)$.

A. INDEX OF REFRACTION

1. Case I

For Case 1 we choose $\alpha(r) = \alpha_0 k_0 r$, or

$$\Theta = \alpha_0 k_0 r \theta \quad (2.5)$$

where α_0 is an arbitrary constant. From equation (2.4) the amplitude is

$$A_p(r, \theta) = F(\theta - \alpha_0 \ln r).$$

Let the function F be multiplied by $\beta_0 k_0$. The amplitude has the final form

$$A_p(r, \theta) = \beta_0 k_0 (\theta - \alpha_0 \ln r) \quad (2.6)$$

where β_0 is an arbitrary constant with units of length. The square of the index of refraction from (2.5) and (2.6) is

$$n^2 = 1 + 2 \left[1 + \frac{1}{2} \left(\frac{\gamma_1}{k_0} \right)^2 \right] \cdot \left\{ 4 \left[1 + \frac{1}{2} \left(\frac{\gamma_1}{k_0} \right)^2 \right]^2 \cdot 2 \left[4 \alpha_0 \theta + 2 \alpha_0^2 + \left(\frac{\gamma_1}{k_0} \right)^4 \right] \right\}^{\frac{1}{2}}. \quad (2.7)$$

The resultant sound speed is shown in Figure 1 for $\alpha_0 = 0.005$ and $C_0 = 1500$ m/s.

2. Case II

For Case II we choose

$$\Theta = \alpha_0 k_0^2 r^2 \theta \quad (2.8)$$

and hence

$$A_p(r, \theta) = \beta_0 k_0 (\theta - \alpha_0 k_0 r). \quad (2.9)$$

The square of the index of refraction is now

$$n^2 = 1 + 2 \left[1 + \frac{1}{2} \left(\frac{\gamma_1}{k_0} \right)^2 \right] - \left\{ 4 \left[1 + \frac{1}{2} \left(\frac{\gamma_1}{k_0} \right)^2 \right]^2 - 2 \left[8\alpha_0 k_0 r \theta + 2\alpha_0^2 k_0^2 r^2 + \left(\frac{\gamma_1}{k_0} \right)^4 \right] \right\}^{\frac{1}{2}}. \quad (2.10)$$

The resulting sound speed is shown in Figure 2 for $\alpha_0 = 4 \times 10^{-7}$ and $C_0 = 1500$ m/s.

B. ENVELOPE FUNCTION

We now have two analytic sound speed fields and the associated acoustic pressure fields derived from the parabolic equation approximation. Considering only $j = 1$, Seigmann et al., (1990) define pressure as

$$\Phi_{PE}(r, \theta, z) = \left(\frac{2}{\pi k_0 r} \right)^{\frac{1}{2}} e^{i(k_0 r - \frac{\pi}{4})} A_p e^{i\theta} \sin(\gamma_1 z) \exp \left\{ -\frac{ik_0 r}{2} \left(\frac{\gamma_1}{k_0} \right)^2 \left[1 - \frac{1}{4} \left(\frac{\gamma_1}{k_0} \right)^2 \right] \right\} \quad (2.11)$$

For Case I, using the amplitude and phase expressed in (2.6) and (2.5), respectively, we obtain

$$\begin{aligned} \Phi_{PE}(r, \theta, z) = & \left(\frac{2}{\pi k_0 r} \right)^{\frac{1}{2}} e^{i(k_0 r - \frac{\pi}{4})} \beta_0 k_0 (\theta - \alpha_0 \ln r) e^{i\alpha_0 k_0 r \theta} \sin(\gamma_1 z) \\ & \times \exp \left\{ -\frac{ik_0 r}{2} \left(\frac{\gamma_1}{k_0} \right)^2 \left[1 - \frac{1}{4} \left(\frac{\gamma_1}{k_0} \right)^2 \right] \right\} \end{aligned} \quad (2.12)$$

For Case II, using (2.8) and (2.9), we get

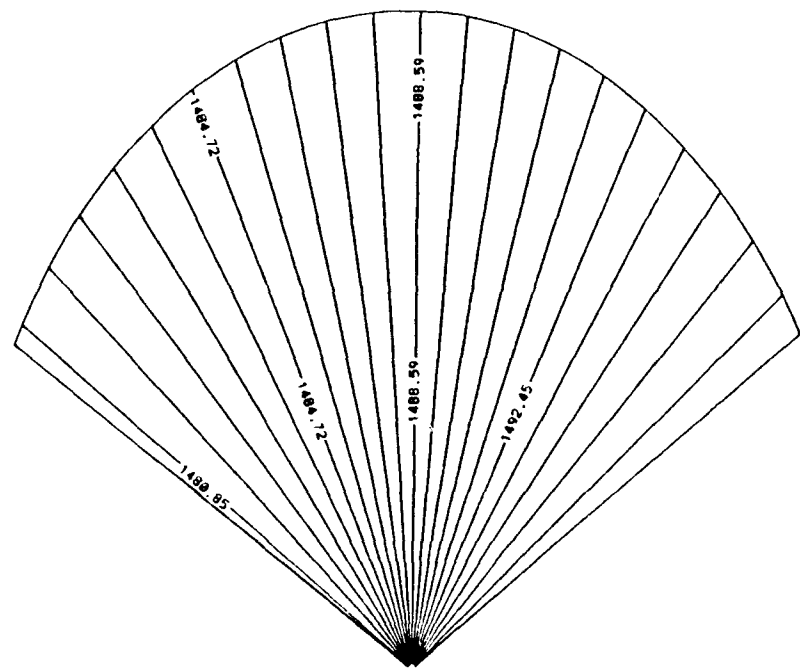


Figure 1. Case I Sound Speed Field for $\alpha_0 = 0.005$ and $C_0 = 1500$ m/s

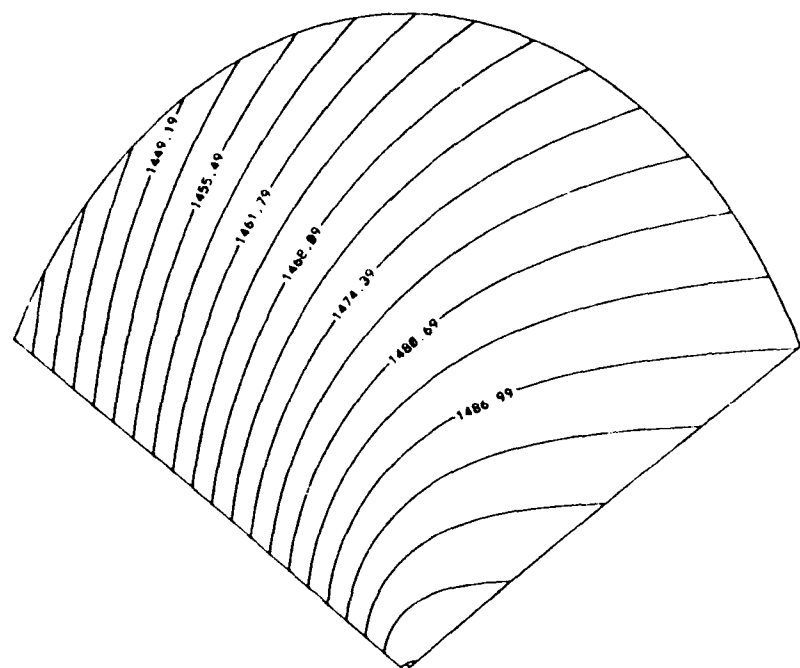


Figure 2. Case II Sound Speed Field for $\alpha_0 = 4 \times 10^{-7}$ and $C_0 = 1500$ m/s

$$\begin{aligned}\Phi_{PE}(r, \theta, z) = & \left(\frac{2}{\pi k_0 r} \right)^{\frac{1}{2}} e^{i \left(k_0 r - \frac{\pi}{4} \right)} \beta_0 k_0 (\theta - \alpha_0 k_0 r) e^{i \alpha_0 k_0^2 r^2 \theta} \sin(\gamma_1 z) \\ & \times \exp \left\{ - \frac{i k_0 r}{2} \left(\frac{\gamma_1}{k_0} \right)^2 \left[1 - \frac{1}{4} \left(\frac{\gamma_1}{k_0} \right)^2 \right] \right\}.\end{aligned}\quad (2.13)$$

In terms of normal modes, pressure can be expressed as

$$\Phi_{NM}(r, \theta, z) = \frac{1}{\sqrt{r}} \sum_n U_n(r, \theta) e^{i \int_0^r k_n(r, \theta) dr} Z_n(z; r, \theta) \quad (2.14)$$

where Z_n is the n^{th} normal mode (eigenmode), k_n is the corresponding horizontal wavenumber (eigenvalue) and U_n is the corresponding slowly varying modulation envelope. See the appendix for details.

Since we are considering depth-invariant sound speed fields, an analytic solution is available for the eigenvalues and eigenmodes. The first mode is

$$Z_1 = \sqrt{\frac{2}{H}} \sin(\gamma_1 z) \text{ where } \gamma_1 = \sqrt{k^2 - k_1^2} = \frac{\pi}{2H}$$

and thus, keeping only the contribution of the first mode, (2.14) becomes

$$\Phi_{NM}(r, \theta, z) = \sqrt{\frac{2}{H}} \frac{1}{\sqrt{r}} U_1(r, \theta) e^{i \int_0^r k_1(r, \theta) dr} \sin(\gamma_1 z). \quad (2.15)$$

The normal mode model entails a numerical calculation of the slowly varying envelope function U_n . Therefore, the quantification of model accuracy can be achieved by comparing the numerical U_n to those derived from the analytic PE solutions. The analytic envelope function $U_1(r, \theta)$ for Case I is derived by equating (2.12) to (2.15). The resulting expression is

$$U_1(r, \theta) = \sqrt{\frac{H}{\pi k_0}} \beta_0 k_0 (\theta - \alpha_0 \ln r) \exp i \left\{ k_0 r \left[1 - \frac{1}{2} \left(\frac{\gamma_1}{k_0} \right)^2 \left(1 - \frac{1}{4} \left(\frac{\gamma_1}{k_0} \right)^2 \right) + \alpha_0 \theta \right] - \int_0^r k_1 dr - \frac{\pi}{4} \right\}^{\frac{1}{2}}. \quad (2.16)$$

where

$$\begin{aligned} k_1^2 &= k^2 - \gamma_1^2 \\ &= k_0^2 \left[n^2 - \left(\frac{\gamma_1}{k_0} \right)^2 \right]. \end{aligned}$$

With the index of refraction n given by (2.7), the range integral of k_1 can be expressed as

$$\int_0^r k_1 dr = k_0 r \left\{ 1 + 2 \left[1 + \frac{1}{2} \left(\frac{\gamma_1}{k_0} \right)^2 \right] - \sqrt{4 \left[1 + \frac{1}{2} \left(\frac{\gamma_1}{k_0} \right)^2 \right]^2 - 2 \left[4 \alpha_0 \theta + 2 \alpha_0^2 + \left(\frac{\gamma_1}{k_0} \right)^4 \right]} - \left(\frac{\gamma_1}{k_0} \right)^2 \right\}^{\frac{1}{2}}.$$

It follows that the analytic envelope function $U_1(r, \theta)$ can be recast as

$$U_1(r, \theta) = \sqrt{\frac{H}{\pi k_0}} \beta_0 k_0 (\theta - \alpha_0 \ln r) e^{i \left(k_0 r \phi - \frac{\pi}{4} \right)} \quad (2.17)$$

where

$$\phi = 1 - \frac{1}{2} \left(\frac{\gamma_1}{k_0} \right)^2 \left[1 - \frac{1}{4} \left(\frac{\gamma_1}{k_0} \right)^2 \right] + \alpha_0 \theta - \left\{ 3 - \sqrt{4 \left[1 + \frac{1}{2} \left(\frac{\gamma_1}{k_0} \right)^2 \right]^2 - 2 \left[4 \alpha_0 \theta + 2 \alpha_0^2 + \left(\frac{\gamma_1}{k_0} \right)^4 \right]} \right\}^{\frac{1}{2}}$$

For Case II, the wave number integral, using (2.10), becomes

$$\int_0^r k_1 dr = k_0 r \left\{ \frac{3}{2} - \frac{1}{2} \left[1 + \frac{1}{2} \left(\frac{\gamma_1}{k_0} \right)^2 \right]^2 + \frac{1}{4} \left(\frac{\gamma_1}{k_0} \right)^4 + \alpha_0 k_0 r \theta + \frac{1}{6} \alpha_0^2 k_0^2 r^2 \right\}.$$

The analytic envelope function U_1 is then

$$U_1(r, \theta) = \sqrt{\frac{H}{\pi k_0}} \beta_0 k_0 (\theta - \alpha_0 k_0 r) e^{i(k_0 r \phi - \frac{\pi}{4})} \quad (2.18)$$

where

$$\begin{aligned} \phi &= 1 - \frac{1}{2} \left(\frac{\gamma_1}{k_0} \right)^2 \left[1 - \frac{1}{4} \left(\frac{\gamma_1}{k_0} \right)^2 \right] + \alpha_0 k_0 r \theta - \frac{1}{k_0 r} \int_0^r k_1 dr \\ &= -\frac{1}{6} \alpha_0^2 k_0^2 r^2. \end{aligned}$$

For Case I we use the analytic envelope function (2.17) to define the initial condition at $r = r_0$ for the numerical model run. The condition is

$$U_1(r_0, \theta) = \sqrt{\frac{H}{\pi k_0}} \beta_0 k_0 (\theta - \alpha_0 \ln r_0) e^{i(k_0 r_0 \phi - \frac{\pi}{4})} \quad (2.19)$$

where

$$\begin{aligned} \phi &= 1 - \frac{1}{2} \left(\frac{\gamma_1}{k_0} \right)^2 \left[1 - \frac{1}{4} \left(\frac{\gamma_1}{k_0} \right)^2 \right] \\ &+ \alpha_0 \theta - \left\{ 3 - \sqrt{4 \left[1 + \frac{1}{2} \left(\frac{\gamma_1}{k_0} \right)^2 \right]^2 - 2 \left[4 \alpha_0 \theta + 2 \alpha_0^2 + \left(\frac{\gamma_1}{k_0} \right)^4 \right]} \right\}^{\frac{1}{2}}. \end{aligned}$$

For Case II we use the analytic envelope function from (2.18) at $r = r_0$. The Case II initial condition is

$$U_1(r_0, \theta) = \sqrt{\frac{H}{\pi k_0}} \beta_0 k_0 (\theta - \alpha_0 k_0 r_0) e^{i(k_0 r_0 \phi - \frac{\pi}{4})} \quad (2.20)$$

where

$$\phi = -\frac{1}{6} \alpha_0^2 k_0^2 r_0^2.$$

III. MODEL RUNS

Our computational domain is in a cylindrical coordinate system. The horizontal range is from 1 km to 100 km. The azimuth range is 30° to 150°. The depth is 4000 m. The domain is the same for both cases.

We use a frequency of 50 Hz and source depth of 1000 m. The reference sound speed is 1500 m/s. We consider mode 1 only. The vertical boundary conditions for the problem are pressure release surface and rigid bottom. Two range and azimuth dependent sound speed fields as presented in the last chapter are used. For Case I sound speed ranges from 1481 m/s to 1496 m/s, varying only in azimuth with a gradient of 0.128 to 0.130 m/s/degree (see Table 1). For Case II sound speed varies in both range and azimuth (see Table 1 again). Here sound speed goes from 1437 m/s to 1500 m/s with a radial gradient of 0.13 to 0.657 m/s/km and an azimuth gradient of 0.004 to 0.431 m/s/degree. Both selections of sound speed fields contain realistic gradients as observed in the ocean.

TABLE 1. THE AZIMUTH AND RADIAL SOUND SPEED VARIATION

Case	Range r[km]	Sound Speed [m/s]			Azimuth Variation $\frac{\partial C}{\partial \theta} \frac{m}{s}/deg$			Radial Variation $\frac{\partial C}{\partial r} \frac{m}{s}/km$		
		θ=30°	θ=90°	θ=150°	θ=30°	θ=90°	θ=150°	θ=30°	θ=90°	θ=150°
I	1	1496	1488	1481	0.1303	0.1289	0.1275	0	0	0
	50	1496	1488	1481	0.1303	0.1289	0.1275	0	0	0
	100	1496	1488	1481	0.1303	0.1289	0.1275	0	0	0
II	1	1500	1500	1499	0.0044	0.0043	0.0043	0.1316	0.3944	0.6482
	50	1493	1480	1468	0.2217	0.2178	0.2142	0.1310	0.3848	0.6221
	100	1487	1462	1437	0.4265	0.4127	0.4001	0.1301	0.3763	0.5992

Eigenmodes and eigenvalues are calculated using finite difference approximations to (A.8) in the appendix with a 40 m vertical grid spacing and a matrix eigenvalue solver.

To obtain the numerical envelope function a first order differential equation ((A.24) in the appendix) is integrated. The radial integration step size is 0.5 km. The 61 integration paths were separated by two degrees.

IV. RESULTS

A. CASE I

In comparing the numerical normal mode (NM) and analytic parabolic equation (PE) results we focus on the slowly varying modulating pressure envelope. The removal of the rapid oscillations, which have wave lengths of order $2\pi/k_0$, makes the displays of results easier to interpret.

Figures 3 and 4 show the amplitude and phase, respectively, of the envelope function calculated by the normal mode model using the Case I sound speed field. Figures 5 and 6 are the amplitude and phase, respectively, of the envelope based on the analytic solution to the parabolic equation.

Figure 7 shows the relative difference, defined as

$$\frac{U_{PE}(\text{analytic solution}) - U_{NM}(\text{numerical solution})}{U_{PE}(\text{analytic solution})}$$

The percent difference is everywhere less than 5%. The difference in NM and PE phase is shown in Figure 8.

Transmission loss at a depth of 1000 m calculated by the NM model, TL_{NM} , is shown in Figure 9. The magnitude of the analytic PE pressure, from (2.12), is

$$|P| = \sqrt{\frac{2}{\pi k_0 r}} A_p \sin(\gamma_j z). \quad (3.1)$$

Substituting (2.6) in (3.1), we get

$$|P| = \sqrt{\frac{2}{\pi k_0 r}} \beta_0 k_0 (\theta - \alpha_0 \ln r) \sin\left(\frac{\pi}{2H} z\right).$$

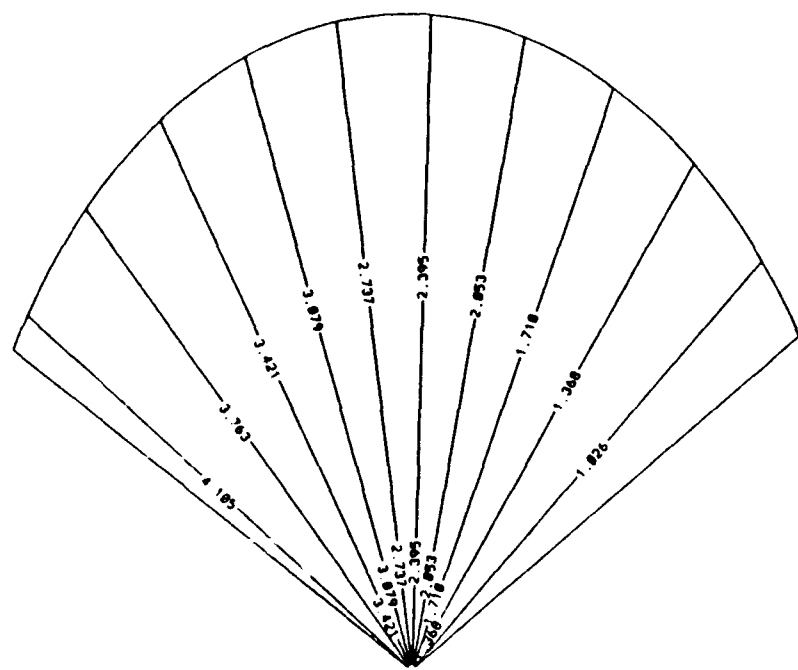


Figure 3. Amplitude of U_{NM} for Case I with $\alpha = 0.005$ and $\beta = 0.1$

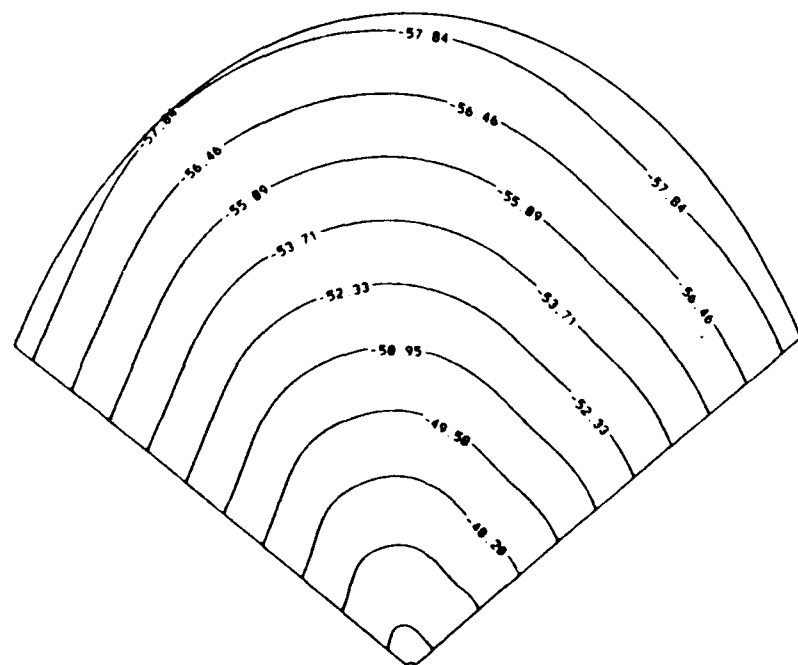


Figure 4. Phase of U_{NM} for Case I with $\alpha = 0.005$ and $\beta = 0.1$

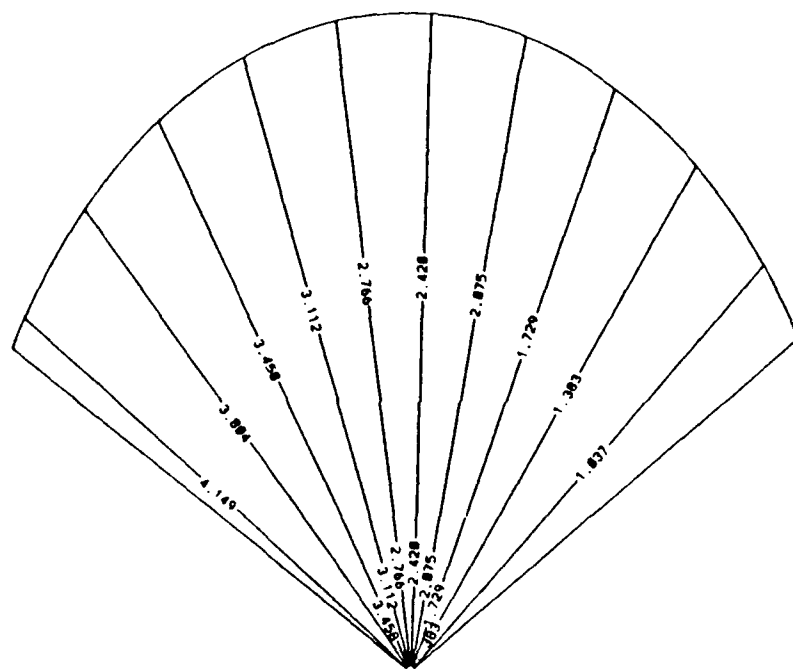


Figure 5. Amplitude of U_{PE} for Case I with $\alpha = 0.005$ and $\beta = 0.1$

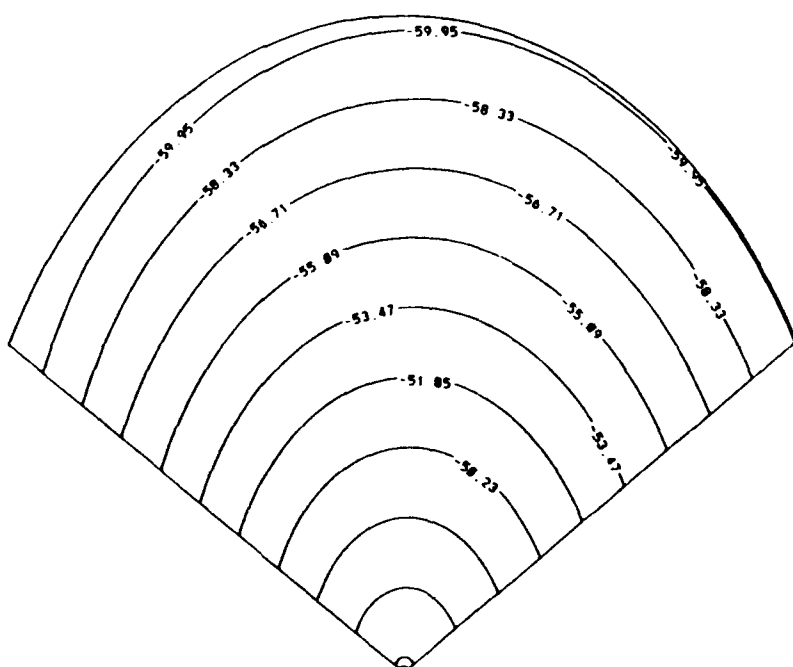


Figure 6. Phase of U_{PE} for Case I with $\alpha = 0.005$ and $\beta = 0.1$

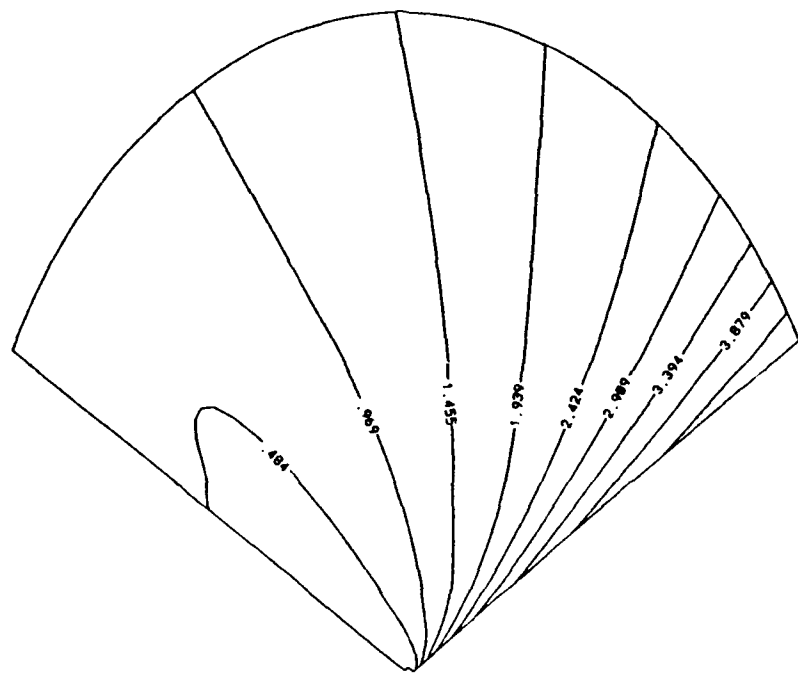


Figure 7. Amplitude Difference in Percent for Case I with $\alpha = 0.005$ and $\beta \approx 0.1$

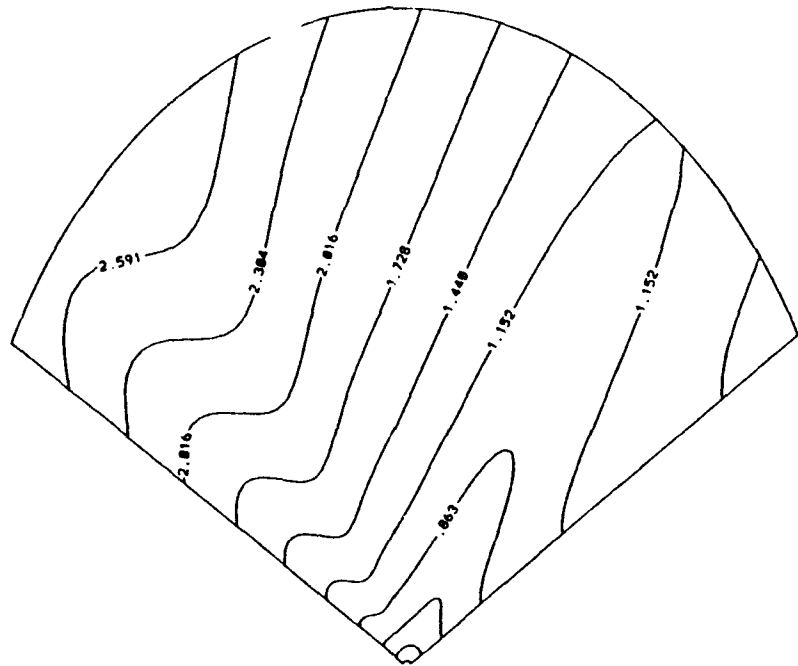


Figure 8. Phase Difference in Degree for Case I with $\alpha = 0.005$ and $\beta = 0.1$

The analytic PE transmission loss TL_{PE} is thus

$$TL_{PE} = -20\log_{10}|P|$$
$$= 10\log_{10}\frac{\pi k_0 r}{2} - 20\log_{10}|\beta_0 k_0(\theta - \alpha_0 \ln r)| - 20\log\left|\sin\frac{\pi}{2H}z\right|.$$

Figure 10 displays TL_{PE} at a depth of 1000m. Both transmission loss results show that the azimuth variation of sound speed produces lower loss at large azimuth angle.

The difference between the analytic PE transmission loss TL_{PE} and the numerical NM transmission loss TL_{NM} is shown in Figure 11. Since the modal transmission loss is a function of amplitude alone this difference has the same shape as the relative error in the amplitude of the envelope function. The difference in transmission loss is everywhere less than 1 dB.

B. CASE II

In the second case, we examined a sound speed field that varies in range and azimuth, closely representing an eddy or ring structure in the real ocean.

Figures 12 and 13 show the amplitude and phase, respectively, of the envelope function U_{NM} from the normal mode model. Note that azimuth variation of the amplitude is larger than range variation. Figures 14 and 15 are the amplitude and phase of the envelope function U_{PE} based on the analytic solution to the wide-angle PE. Figure 16 shows the relative difference of the amplitude. The percent difference is everywhere less than 2%. The difference between the NM and PE phases is shown in Figure 17. The difference of phase is everywhere less than one degree.

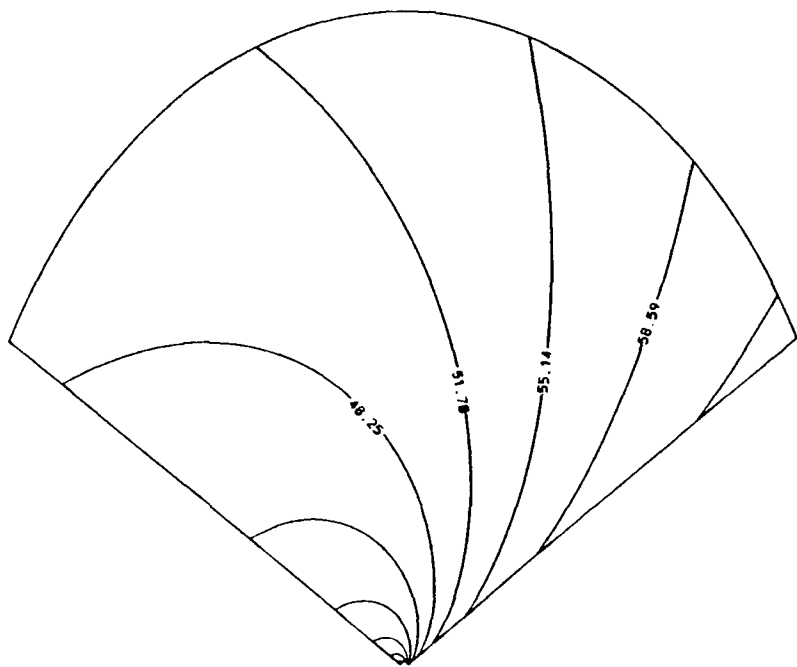


Figure 9. TL_{NM} at a Depth of 1000 m for Case I with $\alpha = 0.005$ and $\beta = 0.1$

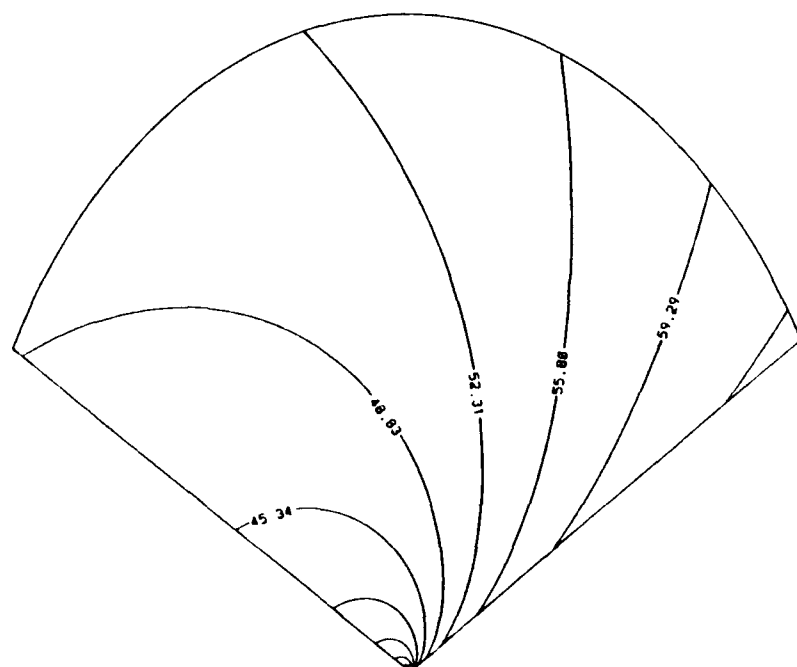


Figure 10. TL_{PE} at a Depth of 1000 m for Case I with $\alpha = 0.005$ and $\beta = 0.1$

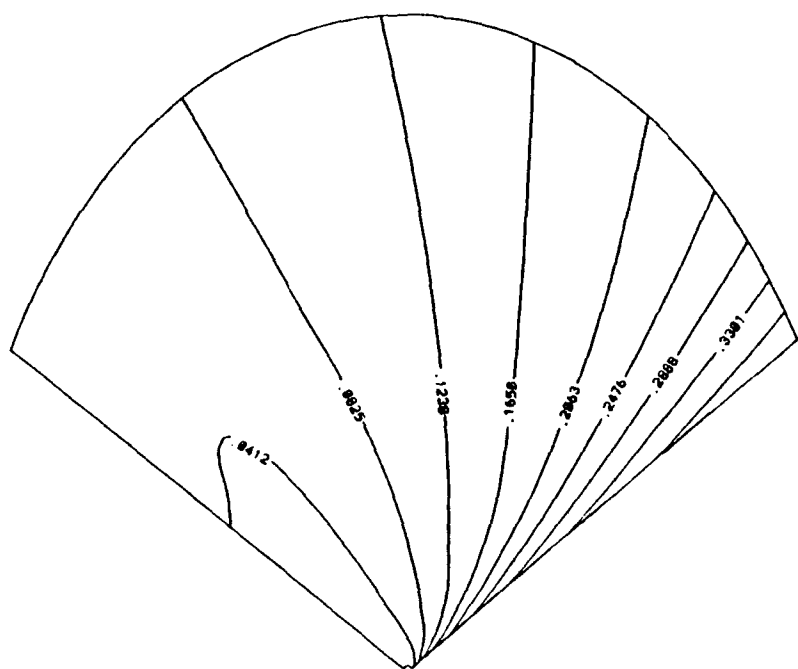


Figure 11. Difference in TL in dB for Case I with $\alpha = 0.005$ and $\beta = 0.1$

The NM and PE transmission losses, TL_{NM} and TL_{PE} , at a depth of 1000 m are shown in Figures 18 and 19, respectively. They are nearly the same as can be seen in Figure 20 where the error is everywhere less than 0.2 dB.

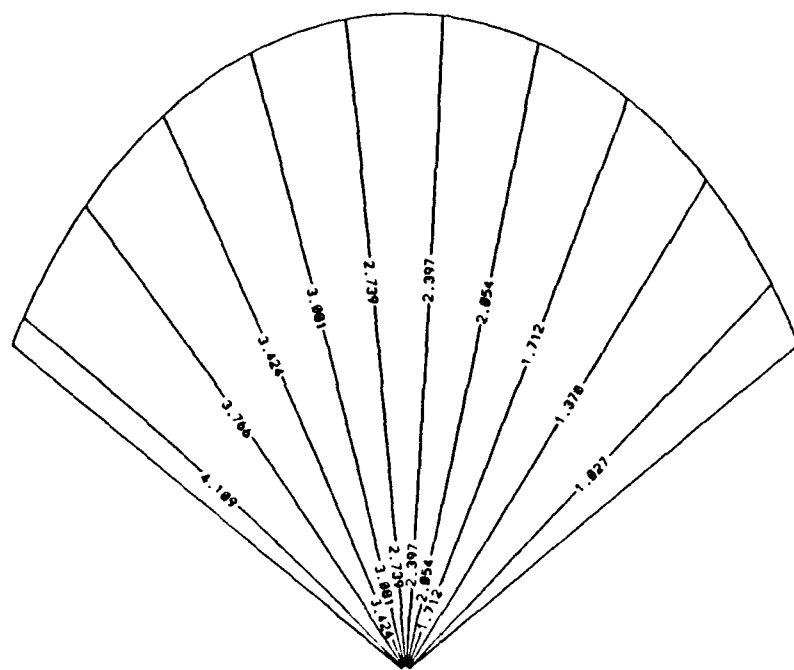


Figure 12. Amplitude of U_{NM} for Case II with $\alpha = 4 \times 10^{-7}$ and $\beta = 0.1$

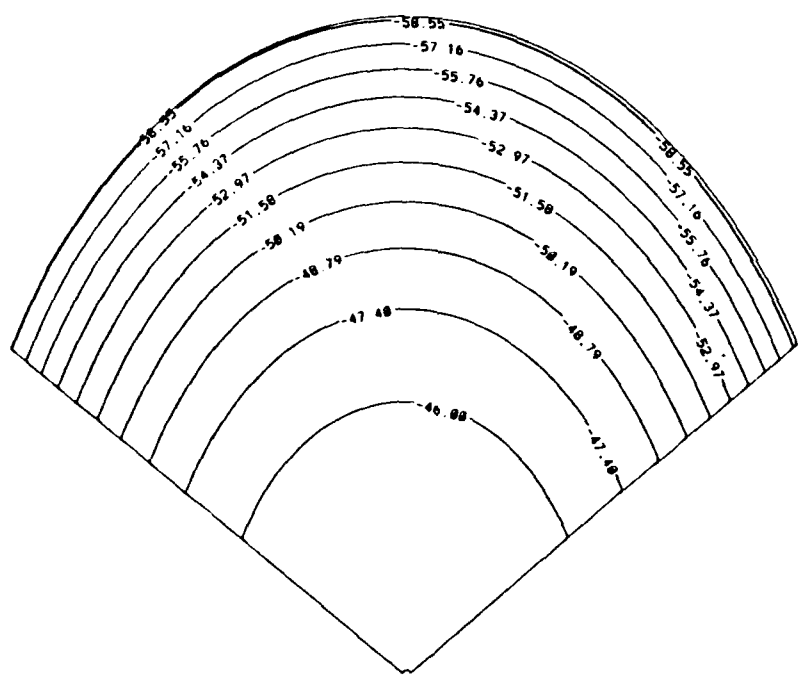


Figure 13. Phase of U_{NM} for Case II with $\alpha = 4 \times 10^{-7}$ and $\beta = 0.1$

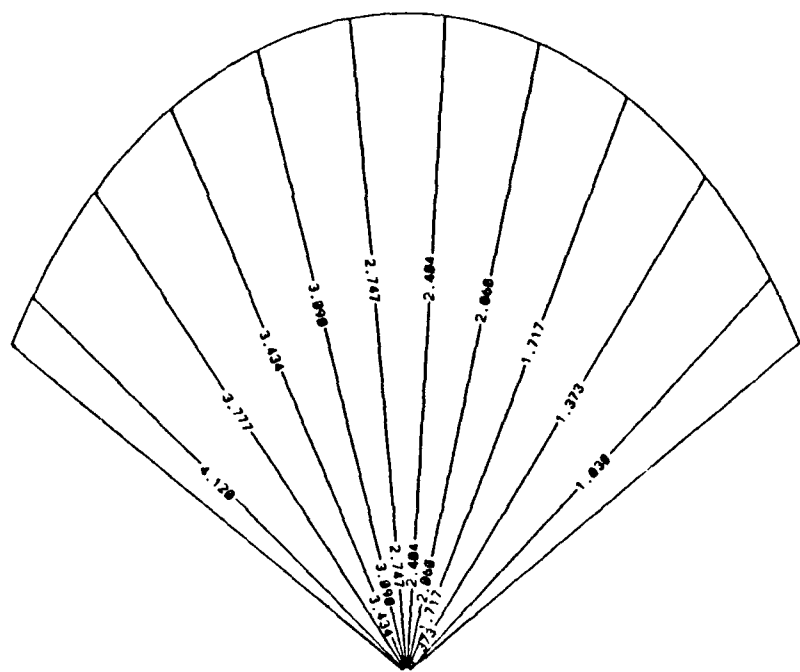


Figure 14. Amplitude of U_{PE} for Case II with $\alpha = 4 \times 10^{-7}$ and $\beta = 0.1$

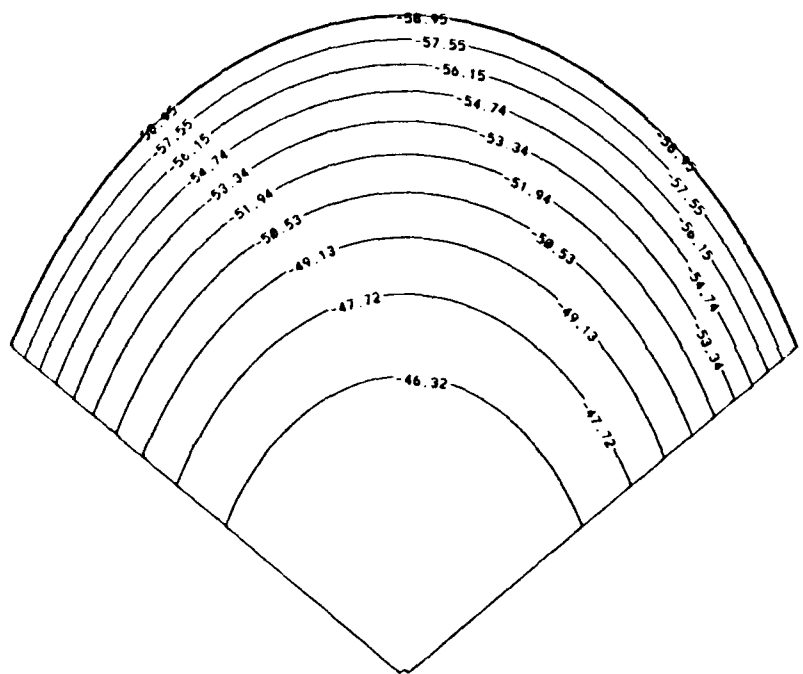


Figure 15. Phase of U_{PE} for Case II with $\alpha = 4 \times 10^{-7}$ and $\beta = 0.1$

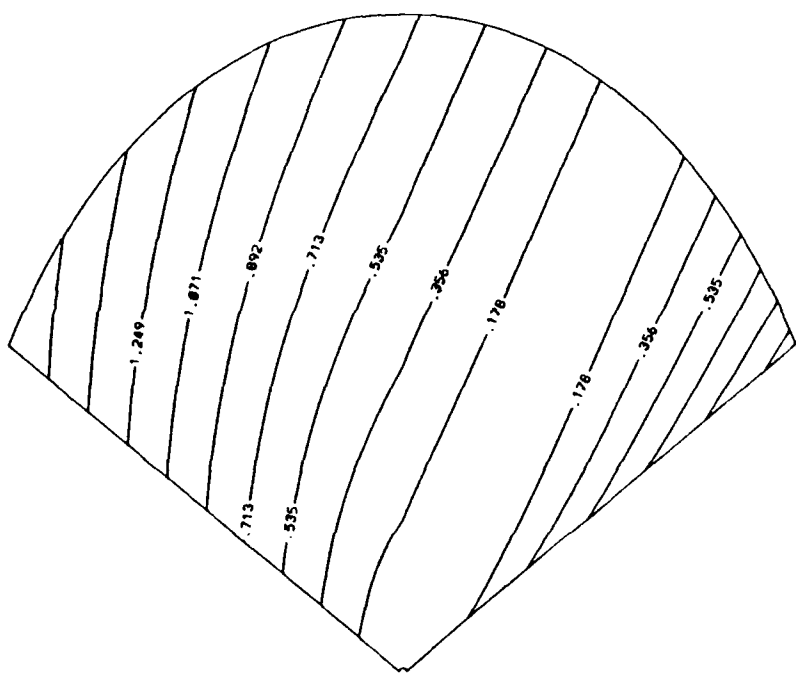


Figure 16. Amplitude Difference in Percent for Case II with $\alpha = 4 \times 10^{-7}$ and $\beta = 0.1$

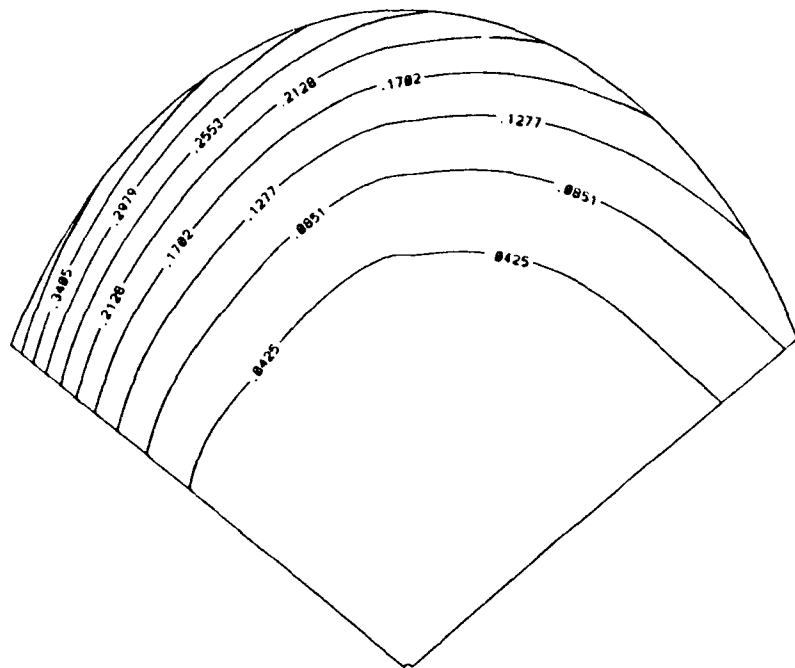


Figure 17. Phase Difference in Degree for Case II with $\alpha = 4 \times 10^{-7}$ and $\beta = 0.1$

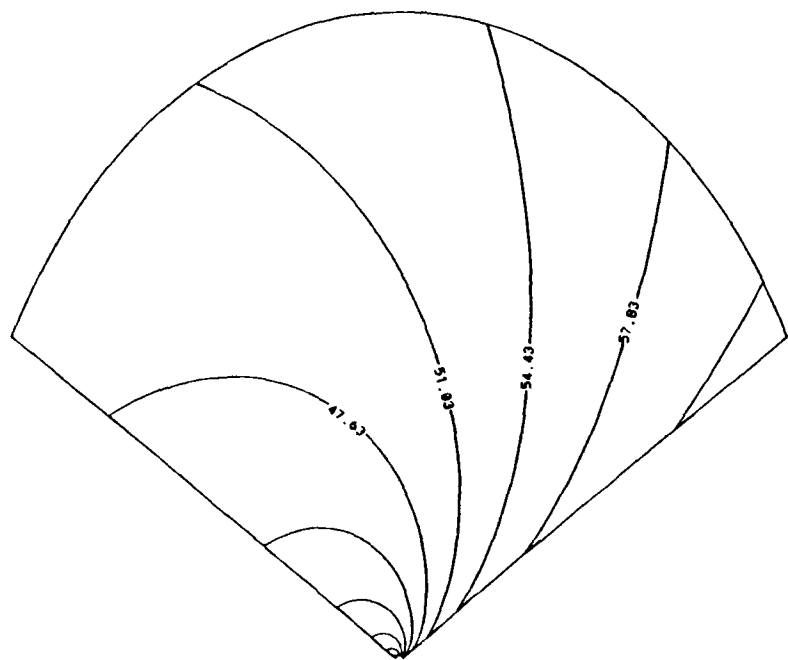


Figure 18. TL_{NM} at a Depth of 1000 m for Case II with $\alpha = 4 \times 10^{-7}$ and $\beta = 0.1$

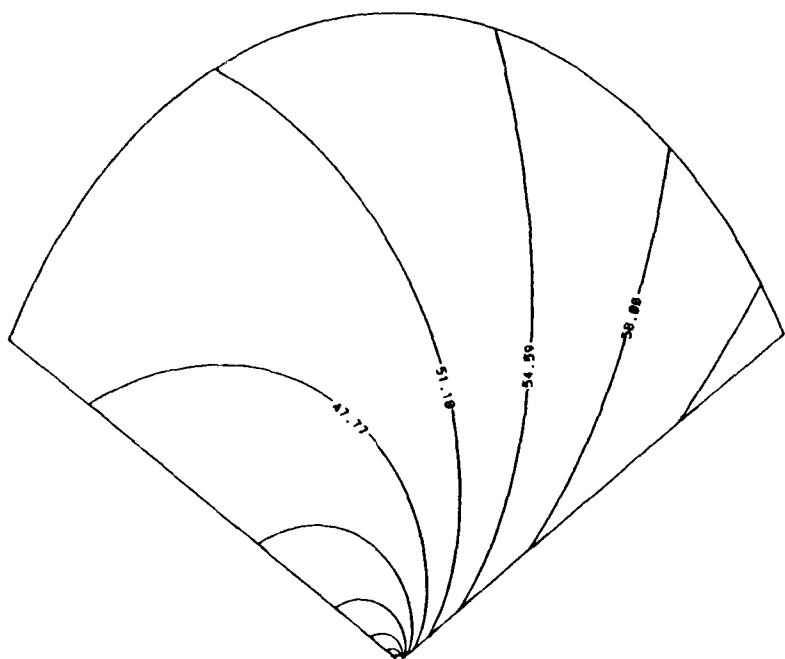


Figure 19. TL_{PE} at a depth of 1000 m for Case II with $\alpha = 4 \times 10^{-7}$ and $\beta = 0.1$

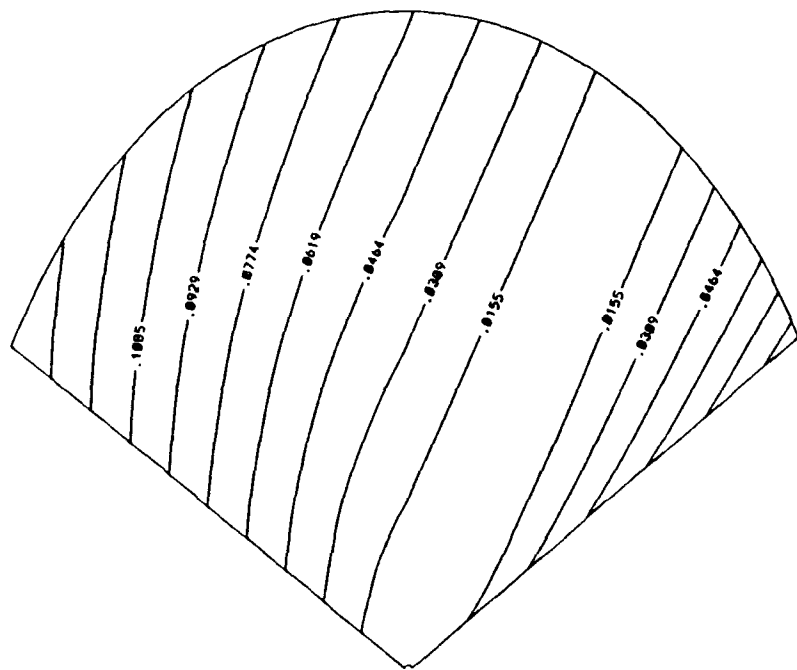


Figure 20. Difference in TL in dB for Case II with $\alpha = 4 \times 10^{-7}$ and $\beta = 0.1$

V. DISCUSSION

In this chapter we address two issues. The first is a quantification of horizontal refraction. The second is an assessment of model accuracy.

A. HORIZONTAL REFRACTION

Critical to this accuracy test is the use of sound speed fields that cause significant horizontal sound refraction. To confirm that the selected sound speed fields do cause significant horizontal refraction, we compare the corresponding $N \times 2D$ NM solutions (the calculation is divided into N vertical slices and a 2D NM model is used in each radial direction) with 3D NM solutions.

The envelope functions of the $N \times 2D$ solutions have been calculated from (A.25) in the appendix. The amplitude of the NM envelope function is the same for both the $N \times 2D$ and 3D solutions in Case I and Case II. However, the phases are different. Figure 21 shows the phase of the $N \times 2D$ envelope function for Case I. The phase is essentially constant at -45° . In Case II, the phase of the envelope function of the $N \times 2D$ solution is also constant and its value is also -45° .

Now let us compare the phases calculated by the $N \times 2D$ method with the phases of the 3D solutions for Case I and Case II, as displayed in Figures 4 and 13, respectively. Both cases show a 13° - 15° phase difference over a range of 100 km, implying that the azimuthal sound speed variation used is large enough to induce sound propagation out of the vertical plane.

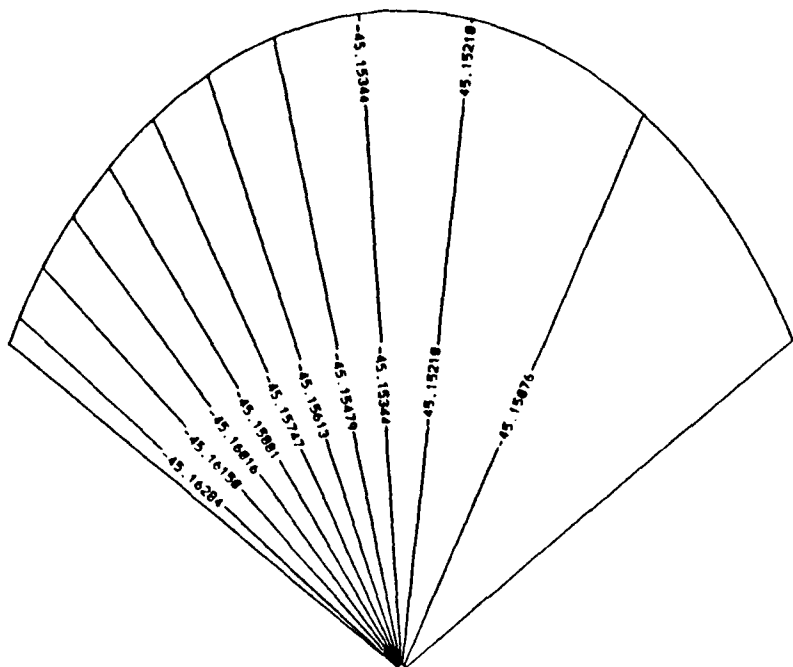


Figure 21. Phase of U_{NM} for $N \times 2D$ for Case I with $\alpha = 0.005$ and $\beta = 0.1$

B. ACCURACY

1. Phase

In this section we discuss the differences between the analytic PE and numerical NM solutions. In Case I, the phase difference between the analytic PE and numerical NM solutions is less than 2.8 degree everywhere. The Case II phase differences between the numerical NM and analytic PE solutions, as shown in Figure 17, is everywhere less than 1 degree. A quantification of the phase differences for the two runs is given in Table 2.

TABLE 2. PHASE DIFFERENCE

Case	PE		Normal Mode NM		Difference PE-NM
	min	max	min	max	max
Case I	-45.15	-60.35	-45.15	-58.92	2.8
Case II	-45.00	-59.04	-45.00	-58.94	0.43

2. Amplitude

Results are shown in Table 3. Envelope amplitude of NM and PE generally agree well with the largest relative difference near 5%. The largest difference occurs in a region that has the largest azimuth gradient in sound speed.

TABLE 3. AMPLITUDE DIFFERENCE

Case	Amplitude of NM		Amplitude of PE		Error Value Difference	Relative Difference [%]
	min	max	min	max	max	max
Case I	0.798	4.22	0.817	4.27	0.038	4.8
Case II	0.851	4.28	0.841	4.28	0.076	1.8

3. Transmission Loss (TL)

The difference in transmission loss between the analytic PE and numerical NM solutions is shown in Table 4. The difference for both cases is everywhere less than half a decibel.

TABLE 4. TRANSMISSION LOSS DIFFERENCE

Case	TL of NM		TL of PE		Difference
	min	max	min	max	max
Case I	28.84	63.31	28.85	63.73	0.43
Case II	28.73	62.75	28.73	62.85	0.15

VI. CONCLUSIONS

In this work we have tested a three-dimensional numerical acoustic coupled mode model. We have sought to describe its accuracy in regard to the modeling of horizontal refraction. In order to test its accuracy, we compared the coupled mode model results with two different analytic solutions to the parabolic wave equation.

We have concentrated on the accuracy of the envelope function and transmission loss calculation. For the sound speed fields described in Table 1, we found that the phase error of the slowly varying envelope function is lower than 2 degrees and that the envelope amplitude agrees to within 5% or better. Our test cases have indicated that the normal mode model agrees closely with the analytic solutions.

We have only used depth-invariant sound speed fields for this test. As a result, the accuracy in modeling mode-mode interactions is not tested here. Future tests should be directed at examining the accuracy of calculating mode-coupling effects using depth varying sound speed fields.

APPENDIX

A. THREE-DIMENSIONAL COUPLED NORMAL MODE METHODS

1. Overview

a. Three-Dimensional (3D) Helmholtz Equation.

The acoustic pressure $P(\bar{r}, t)$ in the ocean is governed by the wave equation:

$$\nabla^2 P(\bar{r}, t) - \frac{1}{C^2(\bar{r})} \frac{\partial^2 P(\bar{r}, t)}{\partial t^2} = 0 \quad (\text{A.1})$$

where $C(\bar{r})$ represents the speed of sound propagation. The cylindrical coordinates are $\bar{r} = (r, \theta, z)$ where r is range, θ is the azimuthal angle measured positive counterclockwise, $-z$ is depth, and ∇^2 is the Laplacian operator in cylindrical coordinates,

$$\nabla^2 = \frac{\partial^2}{\partial r^2} + \frac{1}{r} \frac{\partial}{\partial r} + \frac{1}{r^2} \frac{\partial^2}{\partial \theta^2} + \frac{\partial^2}{\partial z^2}. \quad (\text{A.2})$$

Inclusion of an acoustic source $q(\bar{r}, t)$, modifies Equation (A.1) to

$$\nabla^2 p(\bar{r}, t) - \frac{1}{C^2} \frac{\partial^2 p(\bar{r}, t)}{\partial t^2} = -4\pi q(\bar{r}, t). \quad (\text{A.3})$$

For an acoustic point source located at \bar{r}_0 with time-harmonic circular frequency w , Equation (A.3) becomes

$$\nabla^2 p(\bar{r}, t) - \frac{1}{C^2} \frac{\partial^2 p(\bar{r}, t)}{\partial t^2} = -4\pi \delta(\bar{r} - \bar{r}_0) e^{-iwt}. \quad (\text{A.4})$$

If we let

$$p(\bar{r}, t) = \Phi(\bar{r}) e^{-i\omega t} \quad (A.5)$$

where $\Phi(\bar{r})$ is time-independent, then a Helmholtz equation results:

$$\nabla^2 \Phi(\bar{r}) + k^2(\bar{r}) \Phi(\bar{r}) = -4\pi \delta(\bar{r} - \bar{r}_0) \quad (A.6)$$

where the acoustic wavenumber is $k(\bar{r}) = \frac{w}{c(\bar{r})}$. For $\bar{r} \neq \bar{r}_0$, the Helmholtz Equation is

$$\nabla^2 \Phi(\bar{r}) + k^2(\bar{r}) \Phi(\bar{r}) = 0. \quad (A.6a)$$

b. Coupled Normal-Mode Solution

Adiabatic normal mode theory was applied to a range-dependent medium by Pierce [1965] and Milder [1969]. The pressure field was expressed as a linear combination of the local modes whose coefficients were obtained from a system of decoupled ordinary differential equations. The physics of coupled normal mode theory includes non-adiabaticity and results in a *coupled* system of differential equations. The theory used in the development of the Chiu-Ehret 3D coupled normal mode model follows.

The first step in the development is the expansion of the time-independent pressure component in terms of the local normal modes, i.e.,

$$\Phi(\bar{r}) = \frac{1}{\sqrt{r}} \sum_n P_n(r, \theta) Z_n(z; r, \theta) \quad (A.7)$$

where

Z_n is the n^{th} local normal modes at point (r, θ) .

P_n is the n^{th} mode amplitude function at point (r, θ) .

c. The Local Normal Modes Z_n

The local normal modes obey the following equation:

$$\left[\frac{\partial^2}{\partial z^2} + (k^2 - k_n^2) \right] Z_n = 0 \quad (A.8)$$

where k_n is the horizontal wavenumber associated with the n^{th} mode at each horizontal location.

The idealized upper and lower boundary conditions are

$$Z_n(z = 0; r, \theta) = 0. \quad (A.9)$$

$$\frac{\partial}{\partial z} Z_n(z = -H; r, \theta) = 0. \quad (A.10)$$

where H is the ocean depth. The local normal modes can be normalized according to the orthonormal condition

$$\int_0^H Z_n Z_m dz = \delta_{mn}. \quad (A.11)$$

d. The Mode Amplitude Function P_n

To obtain the governing equation for P_n , substitution of (A.7) in (A.6a) is necessary. The use of (A.8) and the farfield approximation

$$\left[k_m^2 + \frac{1}{4} \frac{1}{r^2} \right] P_m Z_m \sim k_m^2 P_m Z_m \quad (A.12)$$

following the substitution results in the following equation:

$$\begin{aligned} \sum_m \left[Z_m \left(\frac{\partial^2 P_m}{\partial r^2} + \frac{1}{r^2} \frac{\partial^2 P_m}{\partial \theta^2} \right) + 2 \left(\frac{\partial P_m}{\partial r} \frac{\partial Z_m}{\partial r} + \frac{1}{r^2} \frac{\partial P_m}{\partial \theta} \frac{\partial Z_m}{\partial \theta} \right) \right. \\ \left. + P_m \left(\frac{\partial^2 Z_m}{\partial r^2} + \frac{1}{r^2} \frac{\partial^2 Z_m}{\partial \theta^2} \right) + k_m^2 P_m Z_m = 0. \right] \quad (A.13) \end{aligned}$$

The next step is to multiply (A.13) by Z_n and then integrate over z , i.e.,

$$\sum_m \left[\int Z_n Z_m \left(\frac{\partial^2 P_m}{\partial r^2} + \frac{1}{r^2} \frac{\partial^2 P_m}{\partial \theta^2} + k_m^2 P_m \right) dz + 2 \int Z_n \left(\frac{\partial P_m}{\partial r} \frac{\partial Z_m}{\partial r} + \frac{1}{r^2} \frac{\partial P_m}{\partial \theta} \frac{\partial Z_m}{\partial \theta} \right) dz + \int P_m Z_n \left(\frac{\partial^2 Z_m}{\partial r^2} + \frac{1}{r^2} \frac{\partial^2 Z_m}{\partial \theta^2} \right) dz \right] = 0. \quad (\text{A.14})$$

A subsequent application of the orthonormality condition (A.11) on (A.14) gives

$$\begin{aligned} & \left(\frac{\partial^2}{\partial r^2} + k_n^2 + \frac{1}{r^2} \frac{\partial^2}{\partial \theta^2} \right) P_n \\ &= - \sum_m \left[2 \left(\int Z_n \frac{\partial Z_m}{\partial r} dz \right) \frac{\partial P_m}{\partial r} + \frac{2}{r^2} \left(\int Z_n \frac{\partial Z_m}{\partial \theta} dz \right) \frac{\partial P_m}{\partial \theta} + P_m \int Z_n \left(\frac{\partial^2 Z_m}{\partial r^2} + \frac{1}{r^2} \frac{\partial^2 Z_m}{\partial \theta^2} \right) dz \right]. \end{aligned} \quad (\text{A.15})$$

Defining coupling coefficients as

$$\begin{aligned} \gamma_{mn} &= 2 \int Z_n \frac{\partial Z_m}{\partial r} dz \\ \beta_{mn} &= \frac{2}{r} \int Z_n \frac{\partial Z_m}{\partial \theta} dz \\ B_{mn} &= \int Z_n \left(\frac{\partial^2 Z_m}{\partial r^2} + \frac{1}{r^2} \frac{\partial^2 Z_m}{\partial \theta^2} \right) dz, \end{aligned}$$

the coupled system (A.15) can be recast as

$$\left(\frac{\partial^2}{\partial r^2} + k_n^2 + \frac{1}{r^2} \frac{\partial^2}{\partial \theta^2} \right) P_n = - \sum_m \left[\left(\gamma_{mn} \frac{\partial}{\partial r} + \beta_{mn} \frac{1}{r} \frac{\partial}{\partial \theta} \right) + B_{mn} \right] P_m. \quad (\text{A.16})$$

e. The Envelope Functions U_n

Following the work of Chiu and Ehret (1990), the mode amplitude function P_n can be separated into a slowly varying envelope function U_n and a rapidly varying component $e^{i\phi_n(r, \theta)}$, i.e.,

$$P_n = U_n(r, \theta) e^{i\phi_n(r, \theta)} \quad (A.17)$$

$$\phi_n = \int_0^r k_n(r, \theta) dr. \quad (A.18)$$

A substitution of (A.17) into (A.16) yields

$$\left(\frac{\partial^2}{\partial r^2} + k_n^2 + \frac{1}{r^2} \frac{\partial^2}{\partial \theta^2} \right) U_n e^{i\phi_n} = - \sum_m \left[\left(\gamma_{mn} \frac{\partial}{\partial r} + \beta_{mn} \frac{1}{r} \frac{\partial}{\partial \theta} \right) + B_{mn} \right] U_m e^{i\phi_m}$$

which can be expanded as

$$\left[\left(\frac{\partial^2}{\partial r^2} + \frac{1}{r^2} \frac{\partial^2}{\partial \theta^2} \right) + i2k_n \frac{\partial}{\partial r} + \left\{ i \frac{\partial k_n}{\partial r} + \frac{i}{r^2} \frac{\partial^2 \phi_n}{\partial \theta^2} - \frac{1}{r^2} \left(\frac{\partial \phi_n}{\partial \theta} \right)^2 \right\} + \frac{2i}{r^2} \frac{\partial \phi_n}{\partial \theta} \frac{\partial}{\partial \theta} \right] U_n e^{i\phi_n} \quad (A.19)$$

$$= - \sum_m \left[\left(\gamma_{mn} \frac{\partial}{\partial r} + \beta_{mn} \frac{1}{r} \frac{\partial}{\partial \theta} \right) + \left(i\gamma_{mn} k_m + i\beta_{mn} \frac{1}{r} \frac{\partial \phi_m}{\partial \theta} + B_{mn} \right) \right] U_m e^{i\phi_m} \quad (A.20)$$

Dividing (A.20) by $i2k_n e^{i\phi_n}$ gives the governing equation for the envelope:

$$D_n \left(\frac{\partial^2}{\partial r^2} + \frac{1}{r^2} \frac{\partial^2}{\partial \theta^2} \right) U_n + \left(\frac{\partial}{\partial r} + E_n \right) U_n + F_n \frac{1}{r} \frac{\partial}{\partial \theta} U_n = \sum_m \bar{G}_{mn} \cdot \nabla U_m + \sum_m H_{mn} U_m \quad (A.21)$$

where

$$D_n = \frac{-i}{2k_n}$$

$$E_n = \frac{1}{2k_n} \left[\frac{\partial k_n}{\partial r} + \frac{1}{r^2} \frac{\partial^2 \phi_n}{\partial \theta^2} + \frac{i}{r^2} \left(\frac{\partial \phi_n}{\partial \theta} \right)^2 \right]$$

$$F_n = \frac{1}{k_n r} \left(\frac{\partial \phi_n}{\partial \theta} \right)$$

$$\bar{G}_{mn} = \frac{i}{2k_n} \left[\gamma_{mn} \hat{r} + \beta_{mn} \hat{\theta} \right] e^{i(\phi_m - \phi_n)}$$

$$\nabla = \frac{\partial}{\partial r} \hat{r} + \frac{1}{r} \frac{\partial}{\partial \theta} \hat{\theta}$$

$$H_{mn} = \begin{cases} \frac{-1}{2k_n} \left[\gamma_{mn} k_m + \frac{\beta_{mn}}{r} \frac{\partial \phi_m}{\partial \theta} - i B_{mn} \right] e^{i(\phi_m - \phi_n)} & (m \neq n) \\ \frac{i}{2k_n} B_{nn} & (m = n) \end{cases}$$

and \hat{r} and $\hat{\theta}$ are the unit directional vectors in r and θ , respectively.

f. Transmission Loss TL

The mode amplitude function P_n is related to the envelope function U_n and the phase ϕ_n by (A.17). The local normal modes Z_n are solutions to the eigenvalue-eigenfunction problem (A.8)–(A.11). Once P_n and Z_n are computed, pressure can be calculated from the product of P_n and Z_n .

At each point (r, θ, z) , Φ^2 is

$$\Phi^2(r, \theta, z) = [\text{Re}(\Phi)]^2 + [\text{Im}(\Phi)]^2 \quad (\text{A.22})$$

where

$$\text{Re}[\Phi(r, \theta, z)] = \sum_m [\text{Re}(P_m)] \cdot Z_m(z)$$

and

$$\text{Im}(\Phi) = \sum_m [\text{Im}(P_m)] \cdot Z_m(z)$$

In (A.22), Re and Im are used to denote the real and imaginary parts, respectively. Transmission loss can be computed as

$$\text{TL} = -10 \log_{10} \Phi^2(r, \theta, z). \quad (\text{A.23})$$

2. Numerical Solution

a. Numerical Model

To obtain a normal mode solution we must solve the equations for the eigenvalues and eigenmodes (A.8)–(A.11) and the equation for the modulation envelope (A.21). These equations can be solved numerically.

b. The Eigenvalues k_n and the Eigenmodes Z_n

Equation (A.8) is approximated using central finite differencing. This approximation casts (A.8)–(A.10) into a matrix algebra problem. The eigenvalues and the eigenmodes of which can be determined using the iterative QR method (Acton, 1970).

c. The Iterative Method

To obtain the envelope function U_n , we need to solve equation (A.21) which can be rearranged to form a set of first order partial differential equations (PDE) with smaller terms put on the right-hand side. We can solve for U_n in an iterative fashion. The iterative equation is

$$\left[\frac{\partial}{\partial r} + E_n \right] U_n^i - \sum_m H_{mn} U_m^i = -F_n \frac{1}{r} \frac{\partial}{\partial \theta} U_n^{i-1} - D_n \left[\frac{\partial^2}{\partial r^2} + \frac{1}{r^2} \frac{\partial^2}{\partial \theta^2} \right] U_n^{i-1} + \sum_m \bar{G}_{mn} \cdot \nabla U_n^{i-1} \quad (A.24)$$

where U_n^i is the solution at the i^{th} iteration for mode n . This set of first order differential equations is integrated using a Runge-Kutta method of order 5 and 6 (Acton, 1970).

3. The $N \times 2D$ Method

In the $N \times 2D$ method, the sound channel is divided into N vertical slices and the two-dimensional normal mode solution is solved for each slice.

It combines the results in each vertical plane to construct a 3D field. This method provides an approximation to a 3D solution for a 3D sound field.

Thus, in each slice the envelope function U_n is independent of azimuthal variation effects. With the azimuthal terms ignored, the governing equation becomes

$$\left(\frac{\partial}{\partial r} + E_n \right) U_n^i - \sum_m H_{mn} U_m^i = -D_n \frac{\partial}{\partial r^2} U_n^{i-1} + \sum_m \bar{G}_{mn} \nabla U_m^{i-1} \quad (A.25)$$

where

$$D_n = \frac{-i}{2k_n}$$

$$E_n = \frac{1}{2k_n} \frac{\partial k_n}{\partial r}$$

$$\bar{G}_{mn} = \frac{i}{2k_n} \gamma_{mn} \hat{r} e^{i(\phi_m - \phi_n)}$$

$$\nabla = \frac{\partial}{\partial r} \hat{r}$$

$$H_{mn} = \begin{cases} -\frac{1}{2k_n} (\gamma_{mn} k_m + i B_{mn}) e^{i(\phi_m - \phi_n)} & (m \neq n) \\ \frac{i}{2k_n} B_{mn} & (m = n) \end{cases}$$

B. THREE-DIMENSIONAL PARABOLIC WAVE EQUATION

1. Parabolic Wave Equation (PE)

The following work was developed by Tappert (1977) and Lee (1988).

In cylindrical coordinates, the Helmholtz Equation (A.6a) becomes

$$\frac{\partial^2 \Phi}{\partial r^2} + \frac{1}{r} \frac{\partial \Phi}{\partial r} + \frac{1}{r^2} \frac{\partial^2 \Phi}{\partial \theta^2} + \frac{\partial^2 \Phi}{\partial z^2} + k_0^2 n^2 \Phi(r, \theta, z) = 0 \quad (A.26a)$$

where

$$k_0 = w/C_0$$

C_0 is a reference sound speed

w is the harmonic source frequency

n is the index of refraction

$$n = n(r, \theta, z) = C_0 / C(r, \theta, z).$$

The *PE* approximation assumes

$$\Phi(r, \theta, z) = u(r, \theta, z)v(r) \quad (A.26b)$$

where $v(r)$ is rapidly varying and $u(r, \theta, z)$ is a modulation.

By substituting (A.26b) into (A.26a), one obtains

$$\left[\frac{\partial^2 u}{\partial r^2} + \left(\frac{1}{r} + \frac{2}{v} \frac{\partial v}{\partial r} \right) \frac{\partial u}{\partial r} + \frac{1}{r^2} \frac{\partial^2 u}{\partial \theta^2} + \frac{\partial^2 u}{\partial z^2} + k_0^2 n^2 u \right] v + \left[\frac{\partial^2 v}{\partial r^2} + \frac{1}{r} \frac{\partial v}{\partial r} \right] u = 0. \quad (A.26c)$$

If v is determined by

$$\frac{\partial^2 v}{\partial r^2} + \frac{1}{r} \frac{\partial v}{\partial r} + k_0^2 v = 0 \quad (A.27)$$

then u must satisfy

$$\frac{\partial^2 u}{\partial r^2} + \left(\frac{1}{r} + \frac{2}{v} \frac{\partial v}{\partial r} \right) \frac{\partial u}{\partial r} + \frac{1}{r^2} \frac{\partial^2 u}{\partial \theta^2} + \frac{\partial^2 u}{\partial z^2} + k_0^2 (n^2 - 1) u = 0. \quad (A.28)$$

The solution to (A.27) is

$$v(r) = H_0^1(k_0 r) \sim \left(\frac{2}{\pi k_0 r} \right)^{\frac{1}{2}} \exp \left[i \left(k_0 r - \frac{\pi}{4} \right) \right] \quad (A.29)$$

where H_0^1 is a Hankel function of zeroth order.

By substituting (A.29) into (A.28), one gets

$$\left[\frac{\partial^2}{\partial r^2} + 2ik_0 \frac{\partial}{\partial r} + \frac{\partial^2}{\partial z^2} + \frac{1}{r^2} \frac{\partial^2}{\partial \theta^2} + k_0^2(n-1) \right] u = 0 \quad (\text{A.30})$$

which can be factored into

$$\left(\frac{\partial}{\partial r} + ik_0 - ik_0 Q \right) \left(\frac{\partial}{\partial r} + ik_0 + ik_0 Q \right) u = 0 \quad (\text{A.31})$$

where

$$Q = \left[1 + (n^2 - 1) + \frac{1}{k_0^2} \frac{\partial^2}{\partial z^2} + \frac{1}{k_0^2 r^2} \frac{\partial^2}{\partial \theta^2} \right]^{\frac{1}{2}}.$$

Q is called the square root operator. If one considers only outgoing waves, the equation to be solved is

$$\left(\frac{\partial}{\partial r} + ik_0 - ik_0 Q \right) u = 0. \quad (\text{A.32})$$

Let

$$Q = [1 + X + Y]^{\frac{1}{2}} \quad (\text{A.33})$$

so that

$$X = (n^2 - 1) + \frac{1}{k_0^2} \frac{\partial^2}{\partial z^2}$$

$$Y = \frac{1}{k_0^2 r^2} \frac{\partial^2}{\partial \theta^2}$$

and then expand Q in a Taylor series:

$$Q = [1 + X + Y]^{\frac{1}{2}} \approx 1 + \frac{1}{2}X - \frac{1}{8}X^2 + \frac{1}{2}Y + \dots \quad (\text{A.34})$$

Inclusion of the first four terms in the expansion leads to a "wide angle" version of the PE approximation. Substituting (A.34) into (A.32) gives

$$\frac{\partial u}{\partial r} = \frac{ik_0}{2} \left[(n^2 - 1) + \frac{1}{k_0^2} \frac{\partial^2}{\partial z^2} \cdot \frac{1}{4} \left\{ (n^2 - 1) + \frac{1}{k_0^2} \frac{\partial^2}{\partial z^2} \right\}^2 + \frac{1}{k_0^2 r^2} \frac{\partial^2}{\partial \theta^2} \right] u. \quad (\text{A.35})$$

2. The Envelope Function U_p of the Parabolic Equation

Here we present the analytical results of Seigmann et al., (1990). Their development uses the pressure release surface and rigid bottom boundary conditions, i.e.,

$$\begin{aligned} u(r, \theta, z = 0) &= 0 \\ \frac{\partial u}{\partial z}(r, \theta, z = H) &= 0. \end{aligned} \quad (\text{A.36})$$

A solution to equation (A.35) for a depth-independent sound speed field and subject to the boundary conditions stated above can take the following form:

$$u(r, \theta, z) = U_p(r, \theta) \sin(\gamma_j z) \exp \left\{ -\frac{ik_0 r}{2} \left[\frac{\gamma_i}{k_0} \right]^2 \left[1 - \frac{1}{4} \left(\frac{\gamma_j}{k_0} \right)^2 \right] \right\} \quad (\text{A.37})$$

where

$$\gamma_j = \left[j + \frac{1}{2} \right] \frac{\pi}{H},$$

H is the ocean depth, and U_p is the envelope function of the parabolic solution.

By substituting (A.37) into (A.35), one obtains the equation governing U_p :

$$\frac{\partial U_p(r, \theta)}{\partial r} = \frac{ik_0}{2} \left\{ (n^2 - 1) \left[1 + \frac{1}{2} \left(\frac{\gamma_i}{k_0} \right)^2 \right] \cdot \frac{1}{4} (n^2 - 1)^2 \cdot \frac{1}{2} \left(\frac{\gamma_j}{k_0} \right)^4 + \frac{1}{(k_0 r)^2} \frac{\partial^2}{\partial \theta^2} \right\} U_p(r, \theta). \quad (A.38)$$

Letting

$$U_p(r, \theta) = A_p(r, \theta) e^{i\Theta(r, \theta)} \quad (A.39)$$

where both $A_p(r, \theta)$ and $\Theta(r, \theta)$ are real quantities, (A.38) becomes

$$\begin{aligned} \frac{\partial A_p}{\partial r} + i A_p \frac{\partial \Theta}{\partial r} &= \frac{ik_0 A_p}{2} \left\{ (n^2 - 1) \left[1 + \frac{1}{2} \left(\frac{\gamma_j}{K_0} \right)^2 \right] \cdot \frac{1}{4} (n^2 - 1)^2 \cdot \frac{1}{2} \left(\frac{\gamma_j}{k_0} \right)^4 \right\} \\ &+ \frac{i}{2k_0 r^2} \left[\frac{\partial^2 A_p}{\partial \theta^2} + 2i \frac{\partial A_p}{\partial \theta} \frac{\partial \Theta}{\partial \theta} + i A_p \frac{\partial^2 \Theta}{\partial \theta^2} \cdot \left(\frac{\partial \Theta}{\partial \theta} \right)^2 A_p \right] \end{aligned} \quad (A.40)$$

A separation of the real and imaginary parts of (A.40) yields

$$\frac{\partial A_p}{\partial r} + \frac{1}{k_0 r^2} \frac{\partial A_p}{\partial \theta} \frac{\partial \Theta}{\partial \theta} + \frac{A_p}{2k_0 r^2} \frac{\partial^2 \Theta}{\partial \theta^2} = 0 \quad (A.41)$$

$$(n^2 - 1) \left[1 + \frac{1}{2} \left(\frac{\gamma_j}{k_0} \right)^2 \right] \cdot \frac{1}{4} (n^2 - 1)^2 \cdot \frac{1}{2} \left(\frac{\gamma_j}{k_0} \right)^4 = \frac{2}{k_0} \frac{\partial \Theta}{\partial r} + \frac{1}{(k_0 r)^2} \left(\frac{\partial \Theta}{\partial \theta} \right)^2 - \frac{1}{(k_0 r)^2} \frac{1}{A_p} \frac{\partial^2 A_p}{\partial \theta^2} \quad (A.42)$$

Given A_p and Θ , a pressure field is determined, and the index of refraction can be calculated from (A.42). The resultant sound speed field can then be used in the normal mode model.

REFERENCES

Acton, F. S., "Numerical Methods that Work," Harper and Row, Publishers, 1970.

Baer, Ralph N., "Propagation through a Three-dimensional Eddy including Effects on an Array," *J. Acoust. Soc. Am.*, v. 69(1), 1981, pp. 70-75.

Chiu, C. S. and Ehret, L. L., "Computation of Sound Propagation in a Three-dimensionally Varying Ocean: A Coupled Normal Mode Approach," *Computational Acoustics*, v. 1, IMACS, 1990.

Hanish, S., *A Treatise on Acoustic Radiation*, Naval Research Laboratory, Washington, DC, 1989, p. 1-11.

Jones, R. M., Riley, J. P., and Georges, J. M., "HARPO a Versatile Three-Dimensional Hamiltonian Ray-tracing Program for Acoustic Waves in an Ocean with Irregular Bottom," *Wave Prop. Lab. NOAA*, Boulder, CO, p. 457, 1986.

Lee, D., Saad, Y., and Schultz, M. H., "An Efficient Method for Solving the Three-dimensional Wide-angle Wave Equation," *Computational Acoustics*, IMACS, 1988, pp. 75-89.

Lynch, J. F., and Chiu, C. S., "A Report on the 3D Acoustic Working Group Meeting at Long Beach," MA, July 7-8, 1988, WHOL-89-16, June 1989.

Milder, D. M., "Ray and Wave Invariants for SOFAR Channel Propagation," *J. Acoust. Soc. Am.*, v. 46, n. 5, part. 2, 1969, pp. 1259-1263.

Penland, C., "Acoustic Normal Mode Propagation through a Three-dimensional Internal Wave field," *J. Acoust. Soc. Am.*, v. 78, n. 4, 1985, pp. 1356-1365.

Pierce, A. D., "Extension of the Method of Normal Modes to Sound Propagation in an Almost Stratified Medium," *J. Acoust. Soc. Am.*, v. 37, 1965, pp. 19-27.

Seigmann, W. L., Kriegsman, G. A., and Lee, V., "A Wide-angle Three-dimensional Parabolic Wave Equation," *J. Acoust. Soc. Am.*, v. 78, n. 2, 1985, pp. 659-664.

Seigmann, W., Lee, D., and Botseas, G., "Analytic Solution for Testing Accuracy and Azimuthal Coupling in Three-dimensional Acoustic Propagation," *Computational Acoustics*, v. 1, IMACS, 1990.

Tappert, F. D. "The Parabolic Approximation Method," in *Wave Propagation and Underwater Acoustics*, edited by J. B. Keller and J. S. Papadakis (Springer-Verlag, New York, 1977).

INITIAL DISTRIBUTION LIST

1. Defense Technical Information Center 2
Cameron Station
Alexandria, VA 22304-6145
2. Library, Code 52 2
Naval Postgraduate School
Monterey, CA 93943-5002
3. Chairman (Code OC/Co) 1
Department of Oceanography
Naval Postgraduate School
Monterey, CA 93943-5100
4. Professor Ching-Sang Chiu (Code OC/Ci) 1
Department of Oceanography
Naval Postgraduate School
Monterey, CA 93943-5100
5. Professor Laura L. Ehret (Code OC/Eh) 1
Department of Oceanography
Naval Postgraduate School
Monterey, CA 93943-5100
6. Dr. Ding Lee 1
Naval Underwater Systems Center
New London, Ct 06320
7. Dr. William L. Siegmann 1
Rensselaer Polytechnic Institute
Troy, NY 12180-3590
8. Commander Education Division 2
Maritime Staff Office
9-7-45, AKASAKA, MINATO-KU
Tokyo, JAPAN
9. Professor James H. Miller (Code Ee/Mr) 1
Department of Electrical and Computer Engineering
Naval Postgraduate School
Monterey, CA 93943-5100

10. Lieutenant Commander Hiroyuki Ogawa.....2
Maritime Self-Defense Force Service Activity Tokyo
9-7-45, Akasaka, Minato-Ku
Tokyo, JAPAN

11. Dr. James F. Lynch.....1
Dept. of Applied Ocean Physics and Engineering
Woods Hole Oceanographic Institution
Woods Hole, MA 02543